IEEE Access
Multidisciplinary | Rapid Review | Open Access Journal

Received May 6, 2019, accepted May 20, 2019, date of publication May 23, 2019, date of current version June 6, 2019.

Digital Object Identifier 10.1109/ACCESS.2019.2918686

An Optimized Image-Based Visual Servo Control for Fixed-Wing Unmanned Aerial Vehicle Target Tracking With Fixed Camera

LINGJIE YANG, ZHIHONG LIU, XIANGKE WANG, (Senior Member, IEEE), AND YINBO XU
College of Intelligence Science and Technology, National University of Defense Technology, Changsha 410073, China
Corresponding authors: Zhihong Liu (zhliu@nudt.edu.cn) and Xiangke Wang (xkwang@nudt.edu.cn)

ABSTRACT This paper presents an optimized image-based visual servo (IBVS) control scheme for tracking a ground target by using a fixed-wing unmanned aerial vehicle (UAV) with a monocular camera fixed on it. Unlike the widely used rotor UAVs, the fixed-wing UAV has much more dynamical constraints such as it cannot move omni-direction and its minimum speed is limited by the stalling speed. This makes the target tracking problem more challenging. The proposed scheme leverages the image Jacobian matrix to build a connection between the velocity of the feature point and that of the UAV. Afterward, considering the camera is fixed on the body of the UAV, an ''ideal camera'' model is proposed to compensate the shifts of the feature point caused by the changes of the UAV's attitude. Then, an optimized control law without solving the pseudo-inverse of the image Jacobian matrix is proposed with the aid of the least square method from the target center in the image coordinate system. This control law takes the velocity of the feature point as inputs and the yaw angular velocity of the UAV as outputs. The stability of the proposed law is analyzed with the Lyapunov method, showing that the UAV will circle around the ground target asymptotically. Finally, the proposed scheme is evaluated by a hardware-in-the-loop (HIL) simulation based on the Gazebo simulator and the off-the-shelf autopilot hardware.

INDEX TERMS Target tracking, IBVS, fixed-wing UAV, fixed camera, image Jacobian matrix.

I. INTRODUCTION

With the continuous advance of unmanned system technology, researches on UAVs have been extensively carried out in both civilian fields and military fields [1]–[4]. UAVs can be widely used for intelligence, surveillance and reconnaissance (ISR), and even perform some tasks such as landmine detection, border patrol, forest fire rescue which are risky for humans. In particular, target tracking, a mission with real-time and emergency reaction requirements, leverages UAVs increasingly to facilitate the mission execution.

In the last decade, many studies have been presented in the area of target tracking using UAVs. [5]–[9] use adaptive control to handle the parameter uncertainties while performing the target tracking, including the structural uncertainties and unknown external disturbances. This control strategy guarantees the boundedness of the tracking error. Different from the adaptive control, [10]–[15] comprise state and input constraints in the optimization for target tracking by model predictive control. This is important for real systems with physical constraints. Considering the convergence time for the UAV to reach steady state, [16], [17] design the synthesis control to ensure the expected state variables can reach their desired values in short time during tracking. The implementation of synthesis control is via performing the position and attitude tracking control of the dynamical model of the UAV. Based on the motion behavior toward a desired path, [18], [19] construct a vector field. This yields feasible, globally stable paths with guaranteed target stand-off distance bounds.

The relative position of the target to the UAV is an important information for the control of the UAV in target tracking. Most of the aforementioned approaches use GPS to obtain the position information of the UAV. However, it cannot be guaranteed in some specific circumstances, such as battlefield. By contrast, visual servoing offers another option rather than relying on GPS. According to the differences of the feedback information, visual servoing can be divided into

The associate editor coordinating the review of this manuscript and approving it for publication was Chaoyong Li.

three categories, namely, position-based visual servo (PBVS), image-based visual servo (IBVS) and the 2.5D visual servo. PBVS, used to separate visual reconstruction problems from control, is required to estimate the relative pose from the target to the camera [20]–[23]. However, it will generate errors during calibration. In the work of [24]–[27], IBVS is proposed to directly deal with the feature points on images, which avoids the calibration of the camera, whereas encounters the problem of singular value when inversing the image Jacobian matrix. 2.5D visual servo synthesizes PBVS and IBVS by allowing translation control to be done on a 2-dimensional (2D) image while attitude control to be implemented with 3-dimensional (3D) information [28], [29]. 2.5D visual servo can solve the problem of robustness and singularity to some extent, however, it is more sensitive to the noise of pictures than IBVS [30].

Considering difficulties of eliminating the error of calibration and the noise in real images, IBVS has attracted much attention from researchers. Based on rotor UAVs, Falanga *et al.* [31] use IBVS and MPC to make quadrotor with fixed camera fly along circular reference trajectory over the targets, as well as maintaining the targets in the center of the image by adjusting altitude and attitude. Compared with rotor UAVs, target tracking for fixed-wing UAVs are more challenging due to the limit of minimum speed and maneuverability. To solve the problem, Peliti *et al.* [32] use IBVS method to achieve the loitering over a target for the fixed-wing UAV with a gimbaled camera, and Quintero and Hespanha [33] use a fixed-wing UAV equipped with a pan-tilt gimbaled camera to autonomously track a moving ground vehicle. Nevertheless, a pan-tilt gimbaled camera boosts the cost of the UAVs significantly. Thus, tracking a target using the low-cost camera without gimbal is not a trivial problem. However, while using the fixed camera, the optic axis of the camera will dramatically shift due to the changes of the UAV's attitude. To the best of our knowledge, few work is proposed in terms of the target tracking for the fixed-wing UAV with a fixed camera. In particular, Le Bras *et al.* [34] implement the target tracking for a fixed-wing UAV with a fixed camera by IBVS. However, the convergence of the UAV to a cone is based on the 3D inertial reference frame. Besides, the process of obtaining the velocity of the UAV is dependent on the integrating for the flow vector after detecting the landmark.

In this paper, we propose an optimized image-based visual servo control scheme for ground target tracking using fixed-wing UAV with fixed camera. Compared to [34], we control the UAV to circle around the target directly on the 2D image. Simultaneously, we obtain the velocity of the UAV by image Jacobian matrix, which saves the time consumption of integrating. In order to eliminate the dramatical jump of the target feature points under the image coordinate system due to the changes of the UAV's attitude, we import a mechanism called "Ideal Camera" to compensate the feature point's movement. Besides, we build the connection between the velocity of the feature point and that of the UAV by an optimized image Jacobian matrix. Further, we adopt the least square method to obtain the optimal control output of the UAV. The contributions of this paper are summarized as follows:

- We propose a feature point movement compensation mechanism named "Ideal Camera", which effectively handles the jump of feature points caused by the attitude changes of the fixed-wing UAV with fixed camera.
- We propose an optimized image Jacobian matrix that uses centroid coordinates as a single input and avoids solving pseudo-inverse of the image Jacobian matrix. Thus, it is easier to obtain the control output and reduces the time consumption.

The paper is organized as follows. Section II presents the problem of target detection and tracking by fixed-wing UAV with a camera fixed on it. Section III elaborates the details of the control approach and provides the proof for the stability of the control system. Section IV provides the simulation results. Finally, section V is a summary of our work and discussion of future work.

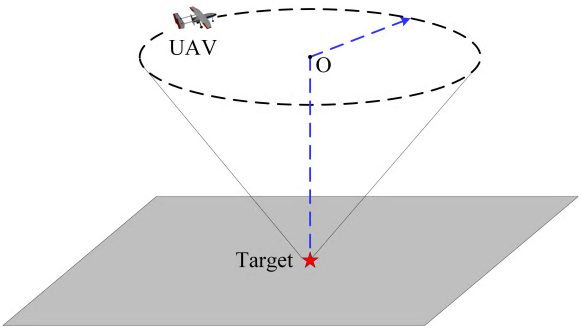

FIGURE 1. The fixed-wing UAV with a fixed camera tracks ground target. Point O is the center of the trajectory.

II. PROBLEM STATEMENT

A. OVERALL FRAMEWORK

Our objective is to design a control strategy that enables the fixed-wing UAV to track a ground target at constant radius, as shown in Fig. 1. The attitude angles of UAV can be expressed by ψ, θ, ϕ (yaw angle, pitch angle and roll angle, respectively).

Remark 1: During the flight of tracking, the fixed-wing UAV flies at constant airspeed of V_t. Besides, the altitude is kept constant as well to obtain an optimal imaging effect.

We use the unicycle model to analyze the kinematics of fixed-wing UAV. We denote by V_x and V_y the linear velocity in the world coordinate system, by u_ψ the input of angular velocity of yaw. Accordingly, we can obtain

$$\begin{cases} V_x = V_t \cdot cos\psi \\ V_y = V_t \cdot sin\psi \\ \dot{\psi} = u_\psi. \end{cases} \tag{1}$$

Remark 2: Fixed-wing UAVs need to reach the minimum speed during flight, thereby cannot hover like rotor UAVs. Besides, the maneuverability is poor since the direction

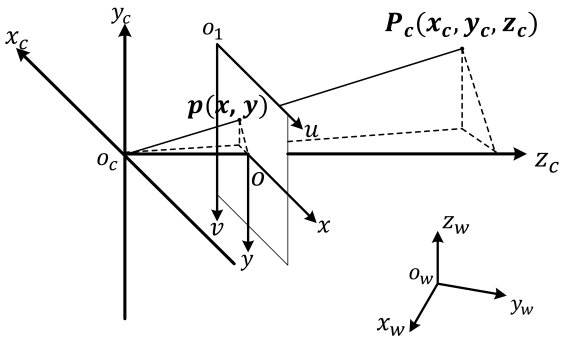

FIGURE 2. The setup of four types of coordinate systems.

of V_t must be consistent with head direction of the UAV without interference. Thus, these dynamic constrains make the target tracking for fixed-wing UAVs more challenging than rotor UAVs.

The image displayed is based on the pinhole imaging principle. For the sake of comparison, the focal plane is often rotated 180 degrees around the optical center of camera. The optical center is on the same side of the target. The model is shown in Fig. 2, and it involves four coordinate systems:

(1) World coordinate system ($\mathbb{F}_w$: o_w-$x_w y_w z_w$)

$\mathbb{F}_w$ is freely defined according to the principle of convenience.

(2) Camera coordinate system ($\mathbb{F}_c$: o_c-$x_c y_c z_c$)

It takes the camera's optical center as the origin, the plane $x_c o_c y_c$ is parallel to the imaging plane, and $\vec{z_c}$ is along the camera's optic axis.

(3) Image coordinate system ($\mathbb{F}_i$: xoy)

It takes symmetry point of the focus of camera relative to the optical center as the origin, plane xoy is the symmetry plane of the imaging plane. The coordinates of points expressed by $\mathbb{F}_c$ satisfy the triangle similarity with those expressed by $\mathbb{F}_i$:

$$\frac{x}{x_c} = \frac{y}{y_c} = \frac{-f}{z_c}, \tag{2}$$

where f is $|o_c o|$ in Fig. 2 and indicates focal length.

(4) Pixel coordinate system ($\mathbb{F}_p$: $uo_1\ v$)

$\mathbb{F}_p$ is coplanar with $\mathbb{F}_i$. o_1 is located in the upper left corner of the image. Besides, its axes are parallel to those in $\mathbb{F}_i$, and directions are the same as well. The relationships among them are shown as follows:

$$\begin{cases} u = u_0 + \dfrac{x}{du} \\ v = v_0 + \dfrac{y}{dv}, \end{cases} \tag{3}$$

where du and dv represent the width and height of each pixel, respectively. u_0 and v_0 represent the coordinates of o in $\mathbb{F}_p$.

B. IMAGE JACOBIAN MODEL

When the pose of the UAV changes, $\mathbb{F}_c$ is also transformed as a certain linear velocity T and angular velocity Ω, and the velocity $\dot{D}$ of the target point $D(x_d, y_d, z_d)$ satisfies the following relationships:

$$\dot{D} = -\Omega \times D - T, \tag{4}$$

in which

$$\Omega = \begin{pmatrix} \omega_x \\ \omega_y \\ \omega_z \end{pmatrix}, \quad T = \begin{pmatrix} v_x \\ v_y \\ v_z \end{pmatrix}.$$

where $\Omega \times D$ can be transformed into a matrix multiplied form, that is:

$$\dot{D} = -sk(D) \cdot \Omega - T, \tag{5}$$

in which

$$sk(D) = \begin{pmatrix} 0 & z_d & -y_d \\ -z_d & 0 & x_d \\ y_d & -x_d & 0 \end{pmatrix}.$$

We denote by $S_c(u_c, v_c)$ the coordinates of the feature point of the target in $\mathbb{F}_p$. Then the coordinates along $\vec{x}$ and $\vec{y}$ in $\mathbb{F}_c$ can be denoted as follows:

$$\begin{cases} u_d = -(u_c - u_0) \\ v_d = -(v_c - v_0). \end{cases} \tag{6}$$

After that, we expand Eq. (5) and substitute Eqs. (2), (3) into it, then get the relationship between feature point S_c and target D in $\mathbb{F}_c$. The velocity of the feature point $\dot{S_c}$ can be represented by

$$\dot{S_c} = J_v \cdot V, \tag{7}$$

in which

$$J_v = \begin{pmatrix} \dfrac{f}{z_d} & 0 & \dfrac{u_d}{z_d} & -\dfrac{u_d v_d}{f} & \dfrac{f^2 + u_d^2}{f} & v_d \\ 0 & \dfrac{f}{z_d} & \dfrac{v_d}{z_d} & -\dfrac{f^2 + v_d^2}{f} & \dfrac{u_d v_d}{f} & -u_d \end{pmatrix},$$

$$V = \begin{pmatrix} T \\ \Omega \end{pmatrix}.$$

The basic form of image-based visual servo control is shown in (7), where J_v is the image Jocabian matrix.

After acquiring the motion velocity V of the target in $\mathbb{F}_c$ by the velocity of the feature point $\dot{S_c}$, it needs to be converted into corresponding motion velocity of the UAV. At this time the transformation relationships between $\mathbb{F}_c$ and $\mathbb{F}_b$ (body coordinate system) needs to be taken into account, which are the rotation matrix of different attitude angles. $\mathbb{F}_b$ of fixed-wing UAV is shown in Fig. 3, in which $\vec{x_b}$ points to the head of UAV, $\vec{z_b}$ is perpendicular to the UAV's body and points to the ground, $\vec{y_b}$ is perpendicular to the plane $x_b o_b z_b$ and points to the right wing.

Rotations around axes in Fig. 3 correspond to three different rotation matrices respectively. With them, the corresponding linear velocity and angular velocity of the UAV in different coordinate systems can be obtained from the current coordinate system.

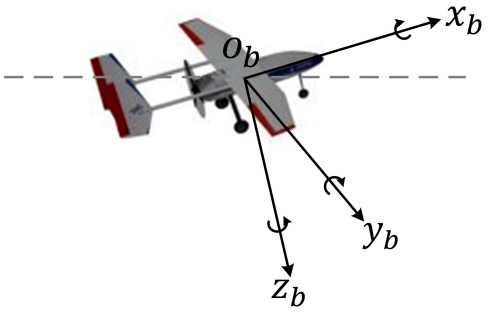

FIGURE 3. Body coordinate system and rotation clockwise around the axes, respectively.

Our work mainly focuses on designing a controller to control the yaw angle of the fixed-wing UAV without GPS after detecting the pixel coordinates of the target, so that the UAV can track the ground target successfully. However, we will encounter a series of challenges summarized as follows:

(1) Since the camera is fixed on the body of the UAV, the heading direction of the camera will be changed as the UAV's attitude changes. Simultaneously, the UAV needs to adjust the attitude to change the flight direction as well. Therefore, how to balance the flight direction and the heading direction of the camera to determine the coordinates of the circling point, which are used to obtain the desired velocity of the feature point in current time, is challenging.

(2) We use the image Jacobian matrix J_v to construct the relationship between the velocity of the feature point and that of the UAV, which are denoted by $\dot{S}_c$ and V in Eq. (7), respectively. The information of $\dot{S}_c$ is needed to obtain the corresponding V, however, the inversion of J_v cannot be performed since the equation expressed by J_v is underactuated. Therefore, how to design the controller to implement the mapping from $\dot{S}_c$ to V is also challenging.

III. CONTROL APPROACH

After analyzing the problem of target tracking for the fixed-wing UAV, we design the controller (Fig. 4) to implement it. Firstly, it is necessary to obtain the attitude (ψ, θ, ϕ), the feature point (u, v) and the speed V_t of the UAV. After that, Attitude compensation is used to obtain the desired velocity of the feature point with the aid of "Ideal Camera" and velocity transformation. Then, the control law is designed based on image Jacobian matrix and the least square method to obtain yaw angular velocity u_ψ of the UAV. Last but not least, the stability of the control law is proved by Lyapunov method.

A. ATTITUDE COMPENSATION USING "IDEAL CAMERA"

We choose the feature point $s(u, v)$ in $\mathbb{F}_p$, and corresponding desired point is s^* (u^*,v^*), then the velocity of the feature point is:

$$\dot{s} = \frac{s^* - s}{T_s}, \tag{8}$$

where T_s represents the sampling period.

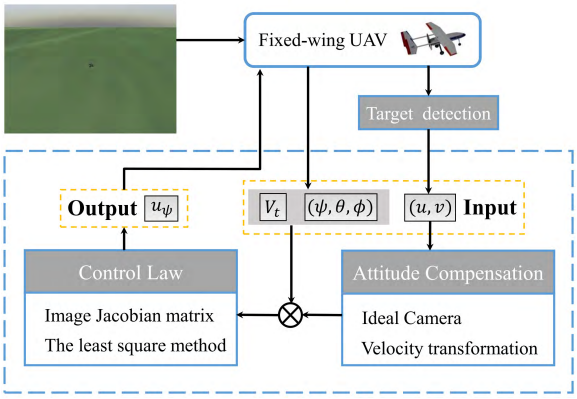

FIGURE 4. The design of the controller.

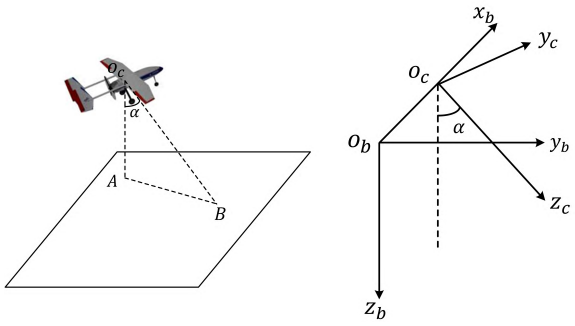

FIGURE 5. Relationship between camera coordinate system and body coordinate system.

As Fig. 5 shows, the camera is mounted on $\vec{x_b}$ of $\mathbb{F}_b$ with its focus at o_c. Therefore, the origin of $\mathbb{F}_c$ is o_c, $\vec{x_c}$ coincides with $\vec{x_b}$ of $\mathbb{F}_b$, $\vec{z_c}$ is perpendicular to $\vec{x_b}$ as well as its angle to $\vec{z_b}$ is α (tilt angle of camera), and $\vec{y_c}$ is determined to make $\mathbb{F}_c$ satisfy the right-hand Cartesian coordinate system.

When the UAV is tracking the ground target, the desired position of the target is set to be the intersection B of the optic axis and ground. At the time the altitude $|o_cA|$ and the circling radius $|AB|$ satisfy the following relationship:

$$tan\alpha = \frac{|AB|}{|o_cA|}. \tag{9}$$

And we need a rotation matrix R_α to implement parallelism between $\mathbb{F}_b$ and $\mathbb{F}_c$:

$$R_\alpha = \begin{pmatrix} 1 & 0 & 0 \\ 0 & cos\alpha & sin\alpha \\ 0 & -sin\alpha & cos\alpha \end{pmatrix}. \tag{10}$$

Since the camera is fixed and when the attitude of the UAV changes, the optic axis of the camera is biased, then Eq. (9) no longer holds. Therefore, we propose a compensation mechanism named "Ideal Camera" to compensate the shifts of the desired feature point caused by the attitude change of the UAV. The "Ideal Camera" model is defined as follows:

Definition 1 (Ideal Camera): When the following three conditions are met at the same time, we call the camera "Ideal Camera":

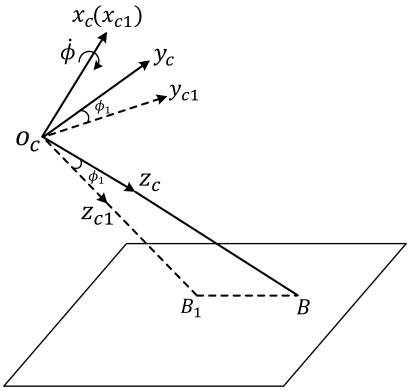

FIGURE 6. Compensation for roll angle.

(1) The relative position of the camera to the UAV remains unchanged;

(2) The centroid of the UAV remains unchanged from current camera to ''Ideal Camera'';

(3) The pitch angle and roll angle of the UAV are both zero in the state.

The purpose that we propose ''Ideal Camera'' is to determine the unique desired feature point on the captured image, even though the attitude of the UAV is dynamically changed. When the UAV's centroid and its yaw angle are determined, we can find the direction of camera's optic axis according to the way of mounting, as the pitch angle and roll angle are both zero. In this case, the intersection of the optic axis and ground is the projection of desired center of the circle trajectory on ground. Considering the rotation order of the attitude angle (first yaw, then pitch, and finally roll), we need to compensate the effects caused by roll angle firstly and then pitch angle.

(1) Compensation for roll angle

As Fig. 6 shows, $\mathbb{F}_c$ in current state is $o_c - x_c y_c z_c$, and the roll angle and pitch angle are ϕ_1 and θ_1, respectively. Then a transformation expressed by rotation matrix R_1 in Eq. (11) around $\vec{x}$ is required if we would like to transform current state S_0 to state S_1 in which the UAV's roll angle is zero.

$$R_1 = \begin{pmatrix} 1 & 0 & 0 \\ 0 & cos\phi_1 & -sin\phi_1 \\ 0 & sin\phi_1 & cos\phi_1 \end{pmatrix} \tag{11}$$

(2) Compensation for pitch angle

When compensating the effect caused by the pitch angle θ_1, we need not only rotation matrix, but also the translation matrix from state S_1 to state S_2 in which the pitch angle is zero as well. Since the origin o_c of $\mathbb{F}_c$ is not consistent with that (o_b) of $\mathbb{F}_b$, which increases not only the complexity of the transformation, but also the difficulty of obtaining the target point's coordinates on the image plane of ''Ideal Camera''. Therefore, we would like to prove the effect caused by the optical center remaining unchanged when computing the coordinates of feature point after pitching is negligible.

As Fig. 7 shows, $o_b x_b$ and $o_b x_b'$ in the left figure represent the $\vec{x}$ of $\mathbb{F}_b$ before and after pitching. $o_c z_c$ and $o_c' z_c'$ indicate

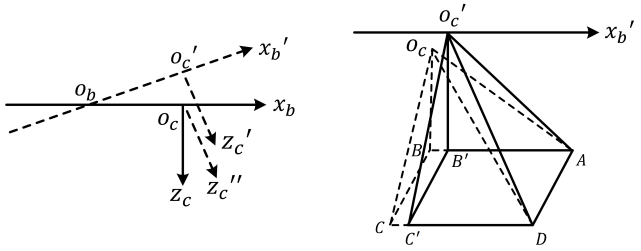

FIGURE 7. Camera imaging when the optical center changes and remains unchanged. The left figure shows the direction of optic axis, where $o_c' z_c'$ is parallel to $o_c z_c''$; the right one shows the 3D projection when the optic axis points to $o_c z_c''$.

the optic axis of the camera before and after tilting. $o_c z_c''$ is parallel to $o_c' z_c'$ and they correspond to $o_c' B'$ and $o_c B$ in the right figure, respectively. We use D to represent the target and denote the coordinates of it by (x, y) in $\mathbb{F}_i$ that $o_c z_c''$ corresponds to, and by (x', y') in $\mathbb{F}_i$ that $o_c' z_c'$ corresponds to. Besides, both image planes are parallel to plane $ABCD$.

Theorem 1: When the optic axis shifts from $o_c z_c$ to $o_c' z_c'$ due to the pitch change of the UAV, it can be considered that the optic axis after pitching is $o_c z_c''$.

Proof: According to the triangle similarity, we have

$$\frac{|x|}{f} = \frac{|AB|}{|o_c B|}, \tag{12}$$

$$\frac{|x'|}{f} = \frac{|AB'|}{|o_c' B'|} = \frac{|AB| - |BB'|}{|o_c B| + \Delta h}, \tag{13}$$

where Δh represents the difference between $o_c B$ and $o_c' B'$ along the optic axis. $|o_c B|$ represents the distance that the optical center reaches the plane including target D, which is perpendicular to optic axis.

Since

$$\Delta h \ll |o_c B|, \quad |BB'| \ll |o_c B|,$$

we have

$$\frac{|AB| - |BB'|}{|o_c B| + \Delta h} \to \frac{|AB|}{|o_c B|}.$$

Therefore we can similarly consider that $x = x'$, and $y = y'$ as well. Equally, the origin of $\mathbb{F}_c$ can be seen unchanged even if the pitch angle changes. Q.E.D.

As Fig. 8 shows, it is necessary to be acted by a rotation matrix R_2 in Eq. (14) when converting state S_1 to state S_2.

$$R_2 = \begin{pmatrix} cos\theta_1 & 0 & sin\theta_1 \\ 0 & 1 & 0 \\ -sin\theta_1 & 0 & cos\theta_1 \end{pmatrix} \tag{14}$$

We denote by $R^{(i-j,\cdot)}$ from the i-th row to j-th row of matrix R, by $R^{(\cdot,i-j)}$ from the i-th column to j-th column of matrix R. By means of compensating for the roll angle and pitch angle, we are able to obtain the image plane corresponding to the ''Ideal Camera'', and therefore the corresponding coordinates of the feature point in state S_2 can be obtained.

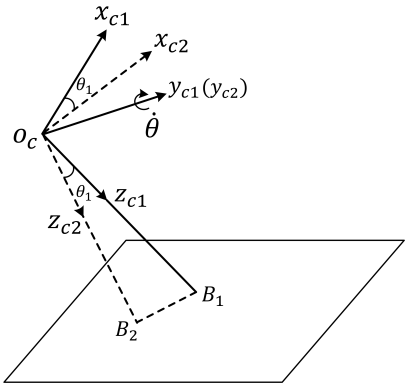

FIGURE 8. Compensation for pitch angle.

Theorem 2: We denote by (x_P, y_P) the coordinates of the feature point in $\mathbb{F}_i$ in state S_0, then the corresponding coordinates (x'_P, y'_P) in $\mathbb{F}_i$ in state S_2 is

$$\begin{pmatrix} x'_P \\ y'_P \end{pmatrix} = \frac{f}{L_1}(R_\alpha^{-1} R_2\, R_1\, R_\alpha)^{(1-2,\cdot)} \begin{pmatrix} x_P \\ y_P \\ -f \end{pmatrix}, \tag{15}$$

in which

$$L_1 = (R_\alpha^{-1} R_2\, R_1\, R_\alpha)^{(3,\cdot)} \begin{pmatrix} x_P \\ y_P \\ -f \end{pmatrix}.$$

Proof: Analyzing the relationship between feature points in state S_0 and state S_2 should start from the target point itself. The mapping of the point on the target to the imaging plane is the intersection of the imaging plane and the line passing through the point and the optical center (the line o_cD in Fig. 7). According to Theorem 1, we believe that the optical center remains unchanged. Then we consider the coordinates representation of the line passing through the target and optical center.

Select a random point $P(X_P, Y_P, Z_P)$ on the line, then X_P, Y_P, Z_P satisfy the following relationships:

$$\frac{X_P}{x_P} = \frac{Y_P}{y_P} = \frac{Z_P}{-f} = k, \tag{16}$$

where k is a non-positive constant, x_P, y_P represent the abscissa and ordinate of the feature point in $\mathbb{F}_i$, then the coordinates of P can be represented by $(kx_P, ky_P, -kf)$. After the compensation of roll and pitch, the corresponding coordinates of P in $\mathbb{F}_c$ of "Ideal Camera" is

$$\begin{pmatrix} X'_P \\ Y'_P \\ Z'_P \end{pmatrix} = R_\alpha^{-1} R_2\, R_1\, R_\alpha \begin{pmatrix} X_P \\ Y_P \\ Z_P \end{pmatrix}. \tag{17}$$

Then the corresponding coordinates of target (x'_P, y'_P) on the image is (X'_P, Y'_P) when $Z'_P = f$. So we have

$$f = k(R_\alpha^{-1} R_2\, R_1\, R_\alpha)^{(3,\cdot)} \begin{pmatrix} x_P \\ y_P \\ -f \end{pmatrix}.$$

After getting k, we substitute it into Eq. (17) and there exist

$$\begin{pmatrix} X'_P \\ Y'_P \end{pmatrix} = k(R_\alpha^{-1} R_2\, R_1\, R_\alpha)^{(1-2,\cdot)} \begin{pmatrix} x_P \\ y_P \\ -f \end{pmatrix}.$$

Q.E.D.

In Eq. (15), the units of x_P, y_P and f are represented in pixels. Therefore, we denote the error of current feature point and desired feature point by $e = (x'_P, y'_P)$ after obtaining the coordinates of the feature point (x'_P, y'_P). In order to start circling for the UAV as quickly as possible, it is necessary to converge the difference between current feature point and desired feature point to zero as quickly as possible. Therefore, we adopt the exponential convergence $\dot{e} = -\lambda e$, where λ is a positive definite matrix of 2×2, so we have

$$\dot{e} = \begin{pmatrix} \dot{u} \\ \dot{v} \end{pmatrix} = -\lambda \begin{pmatrix} x'_P/T_s \\ y'_P/T_s \end{pmatrix}. \tag{18}$$

Eq. (7) illustrates the relationship between the velocity of the feature point and the motion velocity of the target in $\mathbb{F}_c$. Since our objective is to implement the control of fixed-wing UAV, it is necessary to transform the velocity of the target in $\mathbb{F}_c$ to that in $\mathbb{F}_b$, and obtain the control output.

We denote by $\mathbb{F}_{b_2}$ the body coordinate system in state S_2, and by $\mathbb{F}_{b_0}$ the body coordinate system in state S_0. Then we consider the following processes.

(1) Transformation from $\mathbb{F}_c$ to $\mathbb{F}_{b_2}$

When the left figure of Fig. 5 represents the UAV in state S_2, the right one represents the relative position of $\mathbb{F}_c$ to $\mathbb{F}_{b_2}$. We denote the linear velocity and angular velocity of the target in $\mathbb{F}_c$ in state S_0 by

$${}^cV = \begin{pmatrix} {}^cv_x \\ {}^cv_y \\ {}^cv_z \end{pmatrix}, {}^c\Omega = \begin{pmatrix} {}^c\omega_x \\ {}^c\omega_y \\ {}^c\omega_z \end{pmatrix}.$$

Then we need to rotate α counterclockwise around $\vec{x}$ of $\mathbb{F}_c$ to be coincident with $\mathbb{F}_b$, and corresponding rotation matrix is R_α.

Therefore, the linear velocity ${}^{b_2}V$ and angular velocity ${}^{b_2}\Omega$ of the UAV in $\mathbb{F}_{b_2}$ can be expressed as

$$\begin{pmatrix} {}^{b_2}V \\ {}^{b_2}\Omega \end{pmatrix} = \begin{pmatrix} R_\alpha & O_{3\times3} \\ O_{3\times3} & R_\alpha \end{pmatrix} \begin{pmatrix} {}^cV \\ {}^c\Omega \end{pmatrix}. \tag{19}$$

(2) Transformation from angular velocity in $\mathbb{F}_{b_2}$ to that of Euler angles

If the roll angel and pitch angle of the UAV in current state are rotated ϕ and θ around corresponding axis, respectively, the transformation of coordinate system is shown in Fig. 9. Then the corresponding angular velocity of Euler angles can be obtained by projection transformation in the case that the velocity in $\mathbb{F}_{b_0}$ is known.

Angular velocity of Euler angles are represented by

$${}^e\Omega = (\dot{\phi} \quad \dot{\theta} \quad \dot{\psi})^T.$$

In Fig. 9, $o_b - xyz$ represents inertial coordinate system, and we make it yaw ψ to be coincident with $o_b - x_1y_1z_1$ ($\mathbb{F}_{b_2}$),

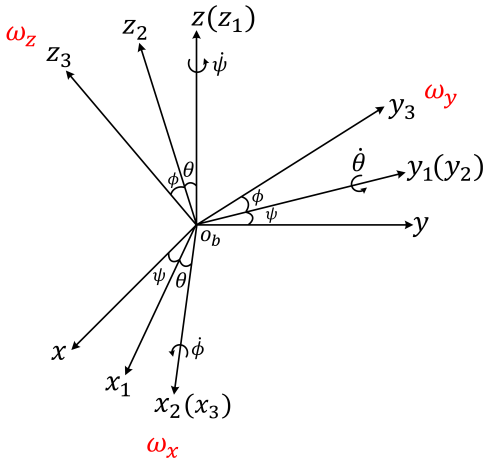

FIGURE 9. Transformation among different angular velocities. ω_x,ω_y and ω_z represent the angular velocities of body coordinate system; $\dot{\phi}$, $\dot{\theta}$ and $\dot{\psi}$ represent the angular velocities of Euler angles.

then pitch θ to be coincident with $o_b - x_2y_2z_2$ ($\mathbb{F}_{b_1}$), finally roll ϕ to be coincident with $o_b - x_3y_3z_3$ ($\mathbb{F}_{b_0}$). Considering the projection of angular velocity in $\mathbb{F}_{b_2}$ from ${}^e\Omega$, we have

$$ {}^e\Omega = \begin{pmatrix} cos\theta & 0 & sin\theta \\ 0 & 1 & 0 \\ 0 & 0 & 1 \end{pmatrix} {}^{b_2}\Omega = R_\theta \cdot {}^{b_2}\Omega, \tag{20} $$

in which

$$ {}^{b_2}\Omega = (\omega_x \ \omega_y \ \omega_z)^T. $$

B. CONTROL LAW DESIGN

We can obtain the flight control output of the fixed-wing UAV directly from the velocity of the feature point by using IBVS method. Eq. (7) shows the relationship between the velocity of the feature point and the motion velocity of the target in $\mathbb{F}_c$. Under the premise of obtaining the former, we can get the desired velocity V by inverting the image Jacobian matrix J_v.

Since $J_v \in R^{2\times 6}$, Eq. (7) is an underactuated equation, and we cannot get V by inverting the image Jacobian matrix directly. A common solution is to reconstruct the image Jacobian matrix with multiple feature points to satisfy $J_v \in R^{i\times 6}(i \geq 6)$. When $i = 6$ and J_v is a non-singular matrix, we can invert it directly; and we can get the pseudo-inverse of J_v by using the least square method when $i > 6$. Then V is obtained.

However, the desired position of the feature points is still agnostic when the fixed-wing UAV starts circling around the target. This makes it difficult to obtain the velocity of the feature points. Therefore, we design a control law by optimizing the control model that the control output of the UAV can be obtained by determining the velocity of the target's centroid only.

Theorem 3: When the fixed-wing UAV circles around the target at uniform speed of V_t at constant altitude, we can obtain the control output of ${}^e\Omega$ just by obtaining the velocity of target's centroid (u_1, v_1). It is

$$ \dot{\psi} = \frac{M_1(\dot{u_1} - \frac{f}{z}V_t) + M_2\dot{v_1}}{M_1^2 + M_2^2}, \tag{21} $$

in which

$$ \begin{aligned} M_1 &= -J_v^{(1,5)} \cdot sin\alpha + J_v^{(1,6)} \cdot cos\alpha, \\ M_2 &= -J_v^{(2,5)} \cdot sin\alpha + J_v^{(2,6)} \cdot cos\alpha. \end{aligned} $$

Proof: Firstly we construct an "Ideal Camera" and define the state as S_2. Then we transform the feature point in current image to that corresponding to state S_2. Finally we can obtain the velocity of the feature point from Eq. (18).

It is known to us that the pitch angle and roll angle are always zero in state S_2 from Definition 1. Therefore, the angular velocity of them are always zero as well. Eq. (20) gives the relationship between the angle velocity of Euler angles and that in $\mathbb{F}_{b_2}$, then we have

$$ \dot{\psi} = {}^{b_2}\omega_z, $$

where ${}^{b_2}\omega_z$ represents the angular velocity around $\vec{z}$ of $\mathbb{F}_{b_2}$.

There exist tilt angle α between $\mathbb{F}_c$ and $\mathbb{F}_b$, and the corresponding rotation matrix is R_α, then we have

$$ \begin{cases} {}^cV = R_\alpha^{-1} \cdot {}^{b_2}V \\ {}^c\Omega = R_\alpha^{-1} \cdot {}^{b_2}\Omega. \end{cases} \tag{22} $$

Since the UAV is flying at uniform speed V_t, there is only linear velocity V_t along $\vec{x}$ in state S_2. And the linear velocity along $\vec{y}$ and $\vec{z}$ are both zero. Besides, there is only non-zero angular velocity ${}^{b_2}\omega_z$ around $\vec{z}$ in the state. Therefore, the velocities in $\mathbb{F}_c$ are

$$ {}^cV = \begin{pmatrix} V_t \\ 0 \\ 0 \end{pmatrix}, \quad {}^c\Omega = \begin{pmatrix} 0 \\ -\dot{\psi} \cdot sin\alpha \\ \dot{\psi} \cdot cos\alpha \end{pmatrix}. \tag{23} $$

Combined with Eq. (7), we have

$$ \begin{pmatrix} M_1 \\ M_2 \end{pmatrix} \dot{\psi} = \begin{pmatrix} \dot{u_1} - \frac{f}{z}V_t \\ \dot{v_1} \end{pmatrix}. \tag{24} $$

As the variable is unique, however, we have two constraints (u_1 and v_1). When the depth z is known, we consider adopting the least square method to obtain the solution, which is

$$ \begin{pmatrix} M_1 & M_2 \end{pmatrix} \begin{pmatrix} M_1 \\ M_2 \end{pmatrix} \dot{\psi} = \begin{pmatrix} M_1 & M_2 \end{pmatrix} \begin{pmatrix} \dot{u_1} - \frac{f}{z}V_t \\ \dot{v_1} \end{pmatrix}. \tag{25} $$

Then Eq. (21) is true. However, if the depth is unknown, we can assume it as a constant. Actually, if the depth can be estimated by some other means, it also tends to a constant when the UAV is flying along the circle trajectory steadily. In our implementation, we set the depth to a constant value, which affects only the radius of the circular trajectory, without affecting the tracking precision of circling around the ground target. Therefore, Eq. (21) is also suitable for the case that the depth is unknown. Q.E.D.

The implementation of the algorithm is shown as Algorithm 1.

Algorithm 1 Using Coordinates of the Feature Point to Obtain Yaw Control of the UAV

Require: coordinates of the feature point

Ensure: angular velocity of yaw

1: **while** discover the target **do**

2: detect the centroid coordinates (x_P, y_P);

3: calculate the rotation matrices R_α, R_1, R_2;

4: obtain the transformed centroid coordinates:

$$\begin{pmatrix} x'_P \\ y'_P \end{pmatrix} = k(R_\alpha^{-1} R_2 R_1 R_\alpha)^{(1-2,\cdot)} \begin{pmatrix} x_P \\ y_P \\ -f \end{pmatrix}$$

5: obtain the velocity of the target:

$$\begin{pmatrix} \dot{u_1} \\ \dot{v_1} \end{pmatrix} = -\lambda \begin{pmatrix} x'_P/T_s \\ y'_P/T_s \end{pmatrix}$$

6: calculate M_1 and M_2:

$$M_1 = -J_v^{(1,5)} \cdot sin\alpha + J_v^{(1,6)} \cdot cos\alpha$$
$$M_2 = -J_v^{(2,5)} \cdot sin\alpha + J_v^{(2,6)} \cdot cos\alpha$$

7: obtain the angular velocity of yaw:

$$\dot{\psi} = \frac{M_1(\dot{u_1} - \frac{f}{z}V_t) + M_2\dot{v_1}}{M_1^2 + M_2^2}$$

8: **end while**

C. STABILITY ANALYSIS

After designing the control law, it is necessary to further verify the stability of it to ensure that the UAV can asymptotically reach convergence state of circling around the target.

When the UAV is flying along the circumference, $\dot{\psi}$ satisfies the following formula:

$$\dot{\psi} = -\frac{g}{V_t} tan\phi. \tag{26}$$

Let

$$\delta = -\frac{g}{V_t} tan\phi - \dot{\psi}, \tag{27}$$

and we can prove the stability of our control law.

Theorem 4: With the controller designed as Eq. (21), when we choose $\dot{\delta}$ as

$$\dot{\delta} = e^T \begin{pmatrix} M_1 \\ M_2 \end{pmatrix} - \beta\delta, \qquad \beta > 0, \tag{28}$$

we are able to make the UAV circle around the ground target with radius unchanged.

Proof: In order to make the UAV track the ground target at constant radius, the following two conditions must be met at the same time:

$$(i) \lim_{t\to\infty} \dot{e} = 0; \quad (ii) \lim_{t\to\infty} \dot{\delta} = 0$$

We consider to use backstepping method to prove that the above two conditions are both met in our control law.

(1) e is convergent

Construct the following Lyapunov function

$$V_1 = \frac{1}{2} e^T e,$$

and combined with Eq. (18), its time derivative can be represented as

$$\dot{V}_1 = e^T \dot{e} = -e^T \lambda e,$$

which indicates that e is convergent.

(2) Both e and δ are convergent

Substitute Eq. (27) into Eq. (24), and we have

$$\dot{e} = -\lambda e + \begin{pmatrix} M_1 \\ M_2 \end{pmatrix} \delta. \tag{29}$$

Then we construct the following Lyapunov-like function

$$V_2 = \frac{1}{2} e^T e + \frac{1}{2}\delta^2,$$

its time derivative can be represented as

$$\dot{V}_2 = -e^T \dot{e} - \delta\dot{\delta}.$$

After substituting Eqs. (28), (29), we have

$$\dot{V}_2 = -e^T \lambda e - \beta\delta^2,$$

which implies that both e and δ are convergent, and our algorithm is asymptotically stable. Q.E.D.

IV. SIMULATION

To evaluate the feasibility of our algorithm, we conduct a series of the HIL simulation experiments. Besides, the experimental results under different circumstances are extensively compared and analyzed.

A. SIMULATION SETUP

Firstly, we use Gazebo as our simulation environment, and add models of fixed-wing UAV and car (acted as the target). Gazebo is a 3D multi-robot simulator with dynamics and offers the ability to accurately and efficiently simulate populations of robots in complex indoor and outdoor environments. It is a well-designed simulator making it possible to rapidly test algorithms, design robots, perform regression testing, and train AI system using realistic scenarios. For the model of fixed-wing UAV, it weights 2.65 kg, the wing surface of it is 0.47 m^2, the wingspan is 2.59 m and the chord length is 0.18 rad. Besides, the tilt angle α is 45 degrees, the horizon of vision is 100 degrees and the image width and height are 960 pixels and 720 pixels, respectively.

Secondly, we use one of the most commonly used off-the-shelf autopilot named Pixhawk in our experiments. It communicates with Gazebo via mavlink protocol, which makes the data of Pixhawk change in real time with the pose transformation of the fixed-wing UAV model, and better simulates the circumstances of the actual flight.

At last, we use QGroundControl (QGC) as the ground station for the purpose of visualizing the current pose of

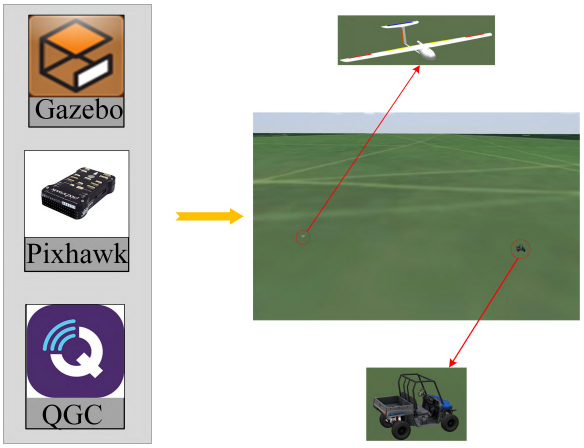

FIGURE 10. The architecture of the HIL simulation. The left part includes the hardware (Pixhawk) and software (Gazebo, QGC) we use; the right part includes the simulation environment and the models of fixed-wing UAV and target (car).

the UAV. It communicates with Pixhawk via mavlink protocol as well, which displays the data of Pixhawk on the screen in real time to generate a flight trajectory.

The setup of simulation is shown as Fig. 10, the right part shows the simulation scene and the models of fixed-wing UAV and car, and the other part includes the hardware and software we use. The detailed implementation process includes: (1) After obtaining the centroid coordinates (u_1, v_1) of the target, the UAV can adjust $\dot{\psi}$ to track the target with the aid of control law. This is the construction of kinematic model for the UAV. (2) Input $\dot{\psi}$, V_t etc. into Pixhawk, then it is able to calculate the power and magnitude of rudder deflection for the UAV, without analyzing the dynamics of the UAV in addition.

B. TRACKING THE STATIC TARGET

In this experiment, we keep the car static on the ground but vary the speed of the UAV to evaluate the tracking performance of our algorithm. Since our experiment aims at making the UAV circle around the target after detecting it, we let the UAV fly to certain position so that it can detect the target and then perform the task of tracking.

During the experiment, we make the flight altitude of the UAV 50 meters, and $\lambda = diag\{0.5, 0.5\}$, $z = 43$ (z was randomly selected). The fixed-wing UAV needs to reach the minimum speed to take off, and it is $10m/s$ in our experiment. Simultaneously, the maximum speed does not exceed $17m/s$ due to the power limit of the UAV's model in Gazebo. Therefore, we considered the following six cases that the velocity of the UAV $V_t = \{11, 12, 13, 14, 15, 16\}(m/s)$.

In Fig. 11, the subfigures from (a) to (f) represent the trajectories that the UAV circles around the target at the speed of $11m/s$ to $16m/s$. In the above six experiments, the relative position of the UAV to the target is almost the same at the start point, and the heading direction of the UAV as well. Due to the difference in the speed of UAV, it will fly around the target with different trajectories, and circle around the target asymptotically. Actually, when V_t becomes larger with other parameters remaining unchanged, $\dot{\psi}$ will become smaller when the UAV is circling around the target according to Eq. (21). Simultaneously, the circular radius R is decided by $R = V_t/\dot{\psi}$, then R will be larger.

As shown in Fig. 12, the distance between the target and the UAV on a horizontal plane can converge to a constant, which verifies the stability of our algorithm.

Fig. 13 shows the image stabilizing precision for the tracking of static target. At the beginning, u and v are far away from zero. By using our target tracking algorithm, the feature point is close to the center of the image gradually. Both u and v converge to zero. Besides, it can be seen from the figure that there is subtle unsmoothness in the red lines, for example, at 32 seconds. This is caused by the deviation of the feature point when detecting the target. Therefore, the results verify the convergence of the feature point's error e.

Fig. 14 displays the tracking performance of the UAV from different perspectives in Gazebo, the figures show that the UAV is rolling right. This indicates that the UAV is circling clockwise around the target. Fig. 15 shows the tracking trajectories of the UAV in QGC, whose results are consistent with Fig. 11.

Besides, the curves do not directly converge to constants smoothly when $V_t = \{15, 16\}(m/s)$ and there are downward overshoots in the beginning. The reason for this is that the optic axis will shift too much if the UAV deflects excessively. This causes the target to be lost as the camera is fixed on the UAV.

When the target is near the right edge of the image, it will be easily lost as the UAV flies forward. To verify the tracking performance of our algorithm for these challenging circumstances, we consider two types of cases as follows: (1) The target lies in the upper right corner of the image. In this situation, the target is not only behind the UAV, but also far from it. (2) The target lies in the bottom right corner of the image. Different from the former, the target is close to the UAV. These two cases are more challenging for the tracking of the ground target, since the UAV has to yaw largely to make the target tend to the center of the image. And the optic axis will shift too much if the yaw angle is very large, which causes the target to be lost.

Fig. 16 shows the tracking performance for the above two cases. The left subfigure simulates the former case and the right one simulates the other. Both trajectories indicate that the UAV will deflect largely at first to keep the feature point away from the image edge, then converge to a circle smoothly. The above results show that our algorithm allows the UAV to maintain good tracking performance regardless of the initial position of the target.

C. TRACKING THE SLOW MOVING TARGET

We run the experiment to evaluate the tracking performance of the UAV on the slow-moving target. In the experiment, we keep the speed of UAV unchanged as $V_t = 14m/s$, but vary the speed of the target. Other parameters are the

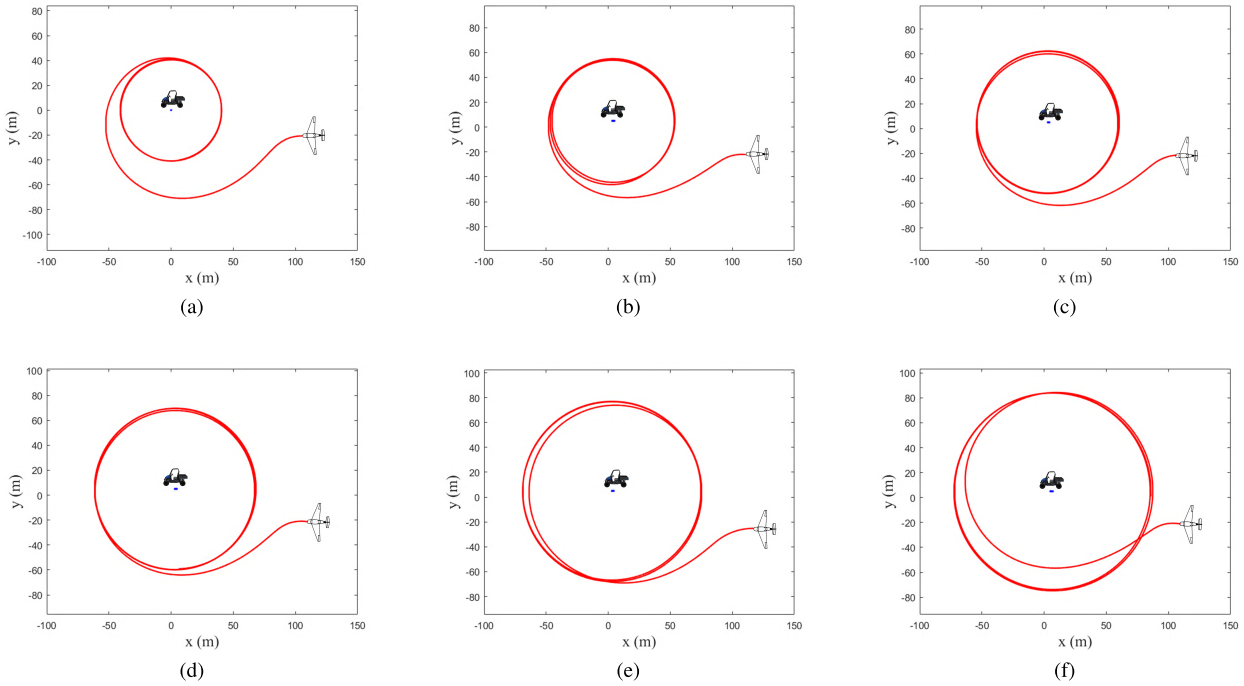

FIGURE 11. Trajectories of the UAV at different speeds when tracking static target. The corresponding speeds from (a) to (f) are 11, 12, 13, 14, 15, 16 (m/s) in turn. The blue point represents the location of car, and the red line represents the trajectory of the UAV.

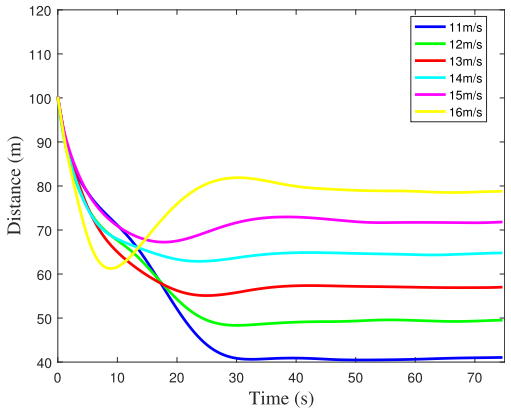

FIGURE 12. Distance between the target and the UAV on horizontal plane under the circumstance that the target is static.

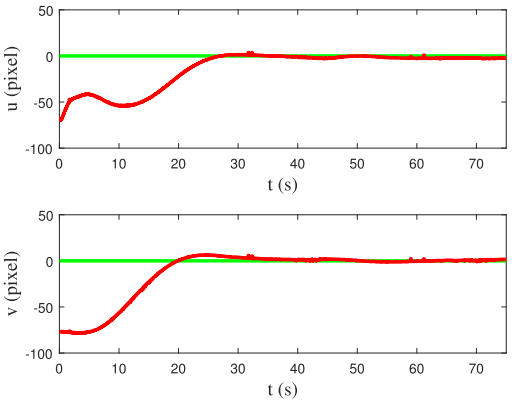

FIGURE 13. Image stabilizing precision for the tracking of static target. The red line represents the changes of the feature point in $\mathbb{F}_i$ (u or v), and the unit is pixel. The green line represents the center of captured image.

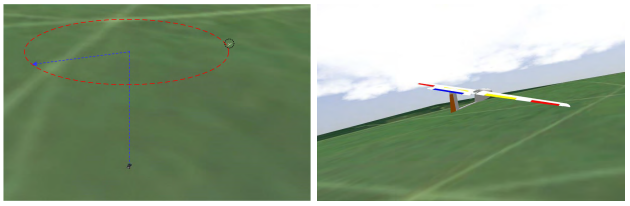

FIGURE 14. The snapshots of the target tracking experiments in Gazebo in different perspectives. The left subfigure shows the tracking trajectory of the UAV around the car.

same as those of the previous experiment. More specifically, we divide the experiment into the following groups: (1) $V_c = 0.5m/s$; (2) $V_c = 1.0m/s$; (3) $V_c = 1.5m/s$.

Fig. 17 shows the results of the experiment. We find that the UAV will make a spiral motion around the target when $V_c \leq 1.5\ m/s$. Besides, with the increasement of the target's speed, the interval between adjacent two rings in the spiral trajectory will become larger.

Fig. 18 shows the distance between the target and the UAV on a horizontal plane, from which we find that the distance will oscillate evenly over time when the target is moving. And the faster the target moves, the greater the amplitude of the oscillation is, since the UAV needs to increase the distance from the target to itself to make the target tend to the center of the image.

Fig. 19 shows the image stabilizing precision for the tracking of slow moving target. When the time is less than $40s$,

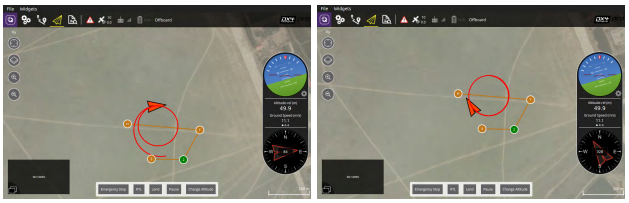

(a) (b)

FIGURE 15. Trajectories of the UAV shown in QGroundControl. The top centers of the images show the mode of the UAV is offboard.

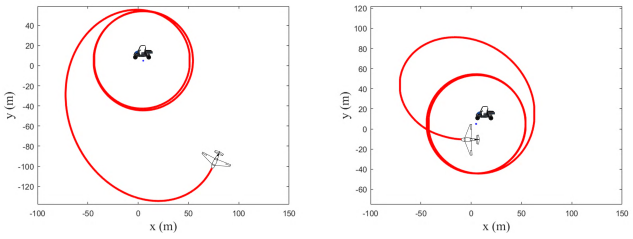

(a) (b)

FIGURE 16. Trajectories of the UAV when tracking the target under two challenging circumstances. The left figure represents the target lies in the upper right of camera field of view while the right one in the bottom right.

the UAV is circling around the static target. However, both u and v will oscillate evenly around zero when the target begins to move. Besides, they will keep opposite movement trend (e.g. u will be close to zero when v stays away from it) to keep the target in the image.

Besides, in order to evaluate the impact of the target's maneuvers on tracking performance, we design the following three maneuvers for the target:

(1) Changing the moving direction drastically

The target moves in a straight line at a constant speed of $V_p = 1.0m/s$ at first. After some time, it suddenly changes the direction drastically and goes on to advance at the same constant speed in the changed direction. The tracking performance is shown as Fig. 20, from which we can see that the UAV is able to track the target by reducing the curvature of the tracking trajectory when the target changes the moving direction drastically.

(2) Moving along a circle

The target moves along a circle at a constant speed of $V_p = 1.0m/s$, and the tracking performance is shown as Fig. 21. From the figure we can know that the tracking trajectory is interlocked with the circle in the shape of spiral. Actually, this situation is similar to that when the target moves in a straight line, except that the target is moving at a constant angular velocity.

(3) Moving along a sinusoid

The target moves along a sinusoid at a constant speed of $V_p = 1.0m/s$, the sinusoid and the tracking trajectory of the UAV are shown as Fig. 22. Compared to Fig. 17 (b) that the target moves in a straight line, we can find that each loop of the tracking trajectory is different in size. This is because the angular velocity of the target is changed under the circumstance, which causes the UAV to increase the angular velocity of yaw somewhere to ensure the target is in view, thereby increasing the curvature of the trajectory.

During the above three experiments, the flight speed of the UAV has been maintained at $V_t = 14m/s$. From these simulation results, we can draw the conclusion that the UAV is able to track the slow moving target even thought the target performs some maneuvers.

D. DISCUSSION

The proposed "Ideal Camera" model is used to obtain the desired feature point of the target by compensating the effect caused by roll and pitch of the fixed-wing UAV. The values of roll angle ϕ_1 and pitch angle θ_1 are provided by IMU (Inertial Measurement Unit) in Pixhawk. However, the measurement errors of both angles will change the position of the desired feature point. Therefore, it is necessary to analyze the tracking performance of the UAV with the measurement errors of ϕ_1 and θ_1.

The map from the detected feature point (u_1, v_1) to the control of yaw $\dot{\psi}$ can be divided into two steps. In step 1, (u_1, v_1) is converted into the desired feature point (u_2, v_2) with the compensation of ϕ_1 and θ_1, and the measurement errors $\Delta\phi$ and $\Delta\theta$ appear in the process. Then step 2 implements the design of yaw control.

Actually, the addition of both $\Delta\phi$ and $\Delta\theta$ will influence the position of (u_2, v_2) directly. After the change of (u_2, v_2), the fixed-wing UAV needs to adjust the heading direction to make the point tend to be stable in the captured image. When (u_2, v_2) fluctuates in a small range with time going by, the UAV will circle around the target at a new constant radius.

Since the centroid coordinates are seen as unchanged before and after $\Delta\phi$ and $\Delta\theta$ are imported, and both of them are small as well, then the position of the target with respect to the intersection of the optic axis and the ground can be considered to be unchanged.

(1) The effect of $\Delta\phi$

As shown in Fig. 23, plane Ω_1 represents ground and is perpendicular to plane Ω_2. OA_3 and OB_3 correspond to the z-axis and optic axis of $\mathbb{F}_{b_0}$ (body coordinate system in state S_0), respectively. After the compensation of ϕ_1, they are transformed into OA_2 and OB_2, and then turned into OA_1 and OB_1 with compensation of θ_1. $\angle B_3OA_3 = \alpha$ (tilt angle of the camera), and we denote the height of camera OC_1 by H. Due to the effect of $\Delta\phi$, OB_3 will become OB_4, where $\angle B_3OB_4 = \Delta\phi$. In other words, the change of circling radius corresponds to B_3B_4, and we denote it by ΔR_ϕ. Then

$$\begin{aligned}\Delta R_\phi &= |A_2B_4| - |A_2B_3| \\ &= |OA_2| \cdot tan(\alpha - \phi - \Delta\phi) - |OA_2| \cdot tan(\alpha - \phi) \\ &= \frac{H}{cos\theta} \cdot (tan(\alpha - \phi - \Delta\phi) - tan(\alpha - \phi)),\end{aligned}$$

where

$$\begin{aligned}tan(\alpha - \phi - \Delta\phi) &= \frac{tan(\alpha - \phi) - tan\Delta\phi}{1 + tan(\alpha - \phi) \cdot tan\Delta\phi} \\ &\approx tan(\alpha - \phi) - tan\Delta\phi \quad (\Delta\phi \to 0).\end{aligned}$$

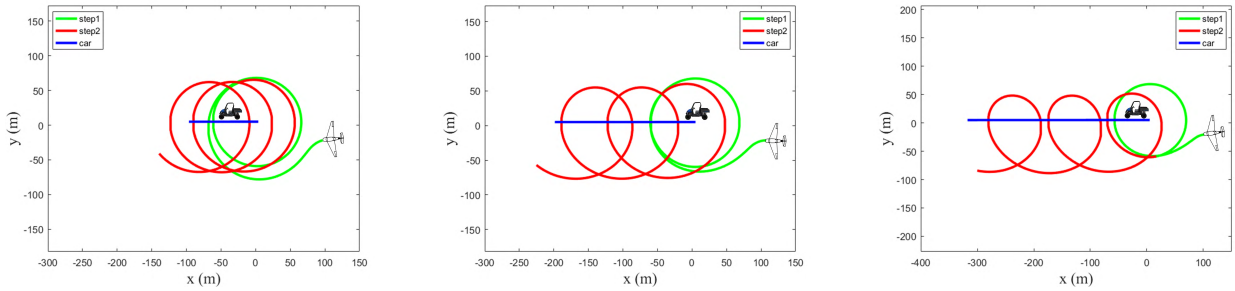

FIGURE 17. Trajectories of the UAV tracking moving target. The speeds of the target from (a) to (c) are $0.5m/s$, $1.0m/s$ and $1.5m/s$. Besides, the green line represents the tracking trajectory of the UAV when the target is static, the red line represents that when the target begins to move, and blue line represents the motion path of the target.

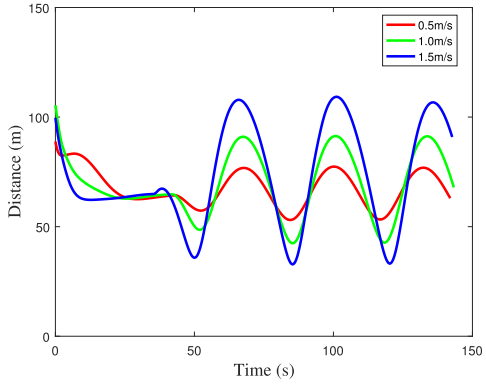

FIGURE 18. Distance between the target and the UAV under the circumstances that the target is moving. The three lines indicate that the speed of the target is $0.5m/s$, $1.0m/s$ and $1.5m/s$, respectively.

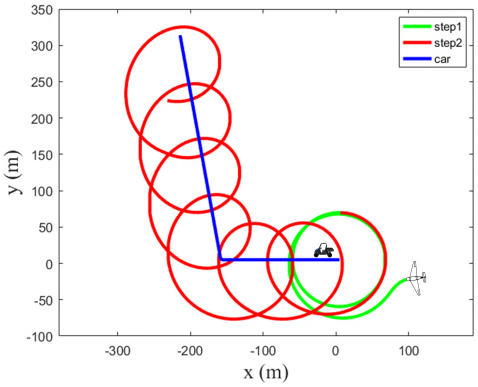

FIGURE 20. Trajectory of the UAV tracking moving target when the target suddenly changes the direction drastically.

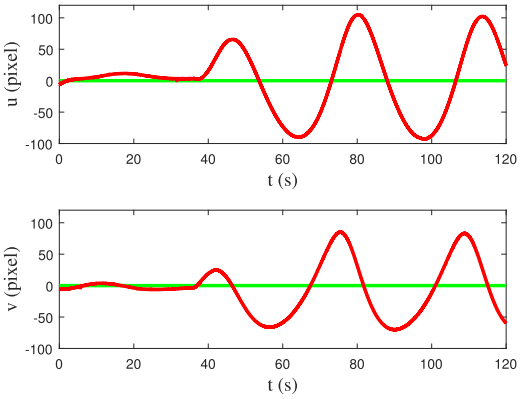

FIGURE 19. Image stabilizing precision for the tracking of the slow moving target.

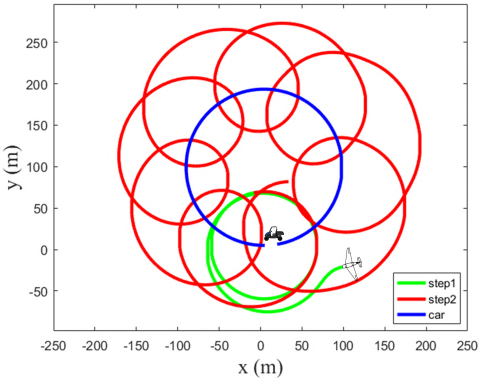

FIGURE 21. Trajectory of the UAV tracking moving target when the target makes a circular motion at a constant speed of 1m/s.

Therefore, we can get the relationship between ΔR_ϕ and $\Delta\phi$ as follows:

$$\Delta R_\phi \approx -\frac{H}{cos\theta} \cdot tan\Delta\phi \quad (\Delta\phi \to 0). \tag{30}$$

(2) The effect of $\Delta\theta$

In Fig. 24, OC_1D_1 and OC_2D_2 correspond to OA_1B_1 and OA_2B_2 in Fig. 23. After the effect of $\Delta\theta$ (θ is negative when the UAV is tilted up in Gazebo), OC_2D_2 becomes OC_3D_3. $\angle C_1OC_2 = \theta$, $\angle C_2OC_3 = \Delta\theta$, $\angle C_2OD_2 = \angle C_3OD_3 = \alpha$. OE_2 and OE_3 are the optic axes of the camera before and after the introduction of $\Delta\theta$. Then the change of circling radius ΔR_θ can be represented as:

$$\begin{aligned}\Delta R_\theta &= |C_3E_3| - |C_2E_2| \\ &= |OC_3| \cdot tan(\alpha - \phi) - |OC_2| \cdot tan(\alpha - \phi) \\ &= \frac{H}{cos(\theta - \Delta\theta)} \cdot tan(\alpha - \phi) - \frac{H}{cos\theta} \cdot tan(\alpha - \phi).\end{aligned}$$

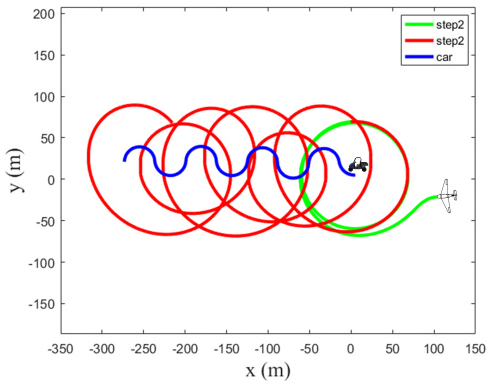

FIGURE 22. Trajectory of the UAV tracking moving target when the target moves along a sinusoid at a constant speed of 1m/s.

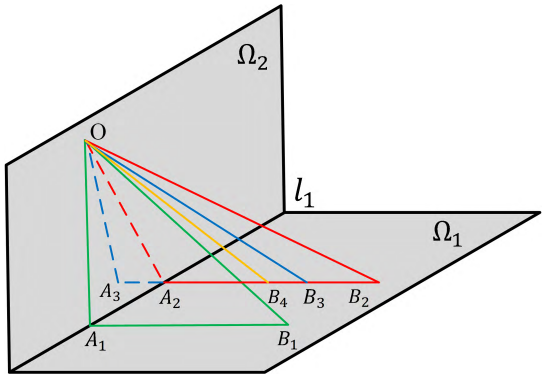

FIGURE 23. The changes of the optic axis after the effect of $\Delta\phi$.

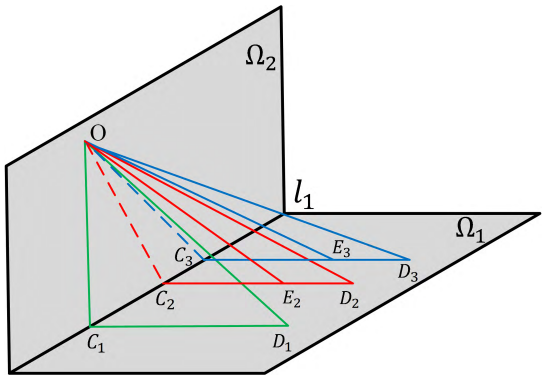

FIGURE 24. The changes of the optic axis after the effect of $\Delta\theta$.

With the aid of Tailor expansion, we have

$$cos(\theta - \Delta\theta) \approx cos\theta + sin\theta \cdot \Delta\theta \quad (\Delta\theta \to 0),$$

then

$$\Delta R_\theta \approx -(\frac{sin\theta}{cos^2\theta} \cdot H \cdot tan(\alpha - \phi)) \cdot \Delta\theta \quad (\Delta\theta \to 0). \quad (31)$$

To verify the aforementioned opinion, we conduct two experiments with the effect of $\Delta\phi$ and $\Delta\theta$, respectively. During the experiments, $V_t = 12m/s$, $z = 43$, $\{\Delta\phi, \Delta\theta\} \in [-5°, 5°]$, and the results are shown in Fig. 25. The figure indicates that ΔR_ϕ (ΔR_θ) is approximately linear with $\Delta\phi$ ($\Delta\theta$), which is consistent with Eq. (30) (Eq. (31)).

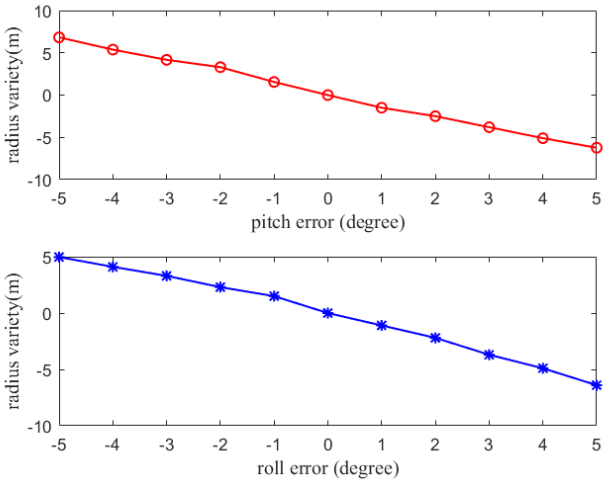

FIGURE 25. The relationship between the pitch/roll error and the change of circling radius.

V. CONCLUSIONS AND FUTURE WORK

In this work, we proposed an optimized image-based visual servo control scheme for ground target tracking using fixed-wing UAV with fixed camera. An "Ideal Camera" model was proposed to compensate the feature point's movement caused by the changes of the UAV's attitude. After that, we used the centroid of the target for control, and avoided the process of the pseudo-inverse of image Jacobian matrix. Moreover, our approach only needed a low-cost camera without any other sensors or GPS, which made it applicable in complex electromagnetic environment. Besides, we built a HIL simulation system, and further proved the feasibility of our method in practical applications through experiments. In the future work, we will solve the problem of tracking fast-moving target by fixed-wing UAV, and improve the stability of our control algorithm under the wind disturbance conditions. The flight tests of the control scheme is also on the way.

REFERENCES

[1] C. Stöcke, R. Bennett, F. Nex, M. Gerke, and J. Zevenbergen, "Review of the current state of UAV regulations," *Remote Sens.*, vol. 9, no. 5, p. 459, May 2017.

[2] L. Tang and G. Shao, "Drone remote sensing for forestry research and practices," *J. Forestry Res.*, vol. 26, no. 4, pp. 791–797, Dec. 2015.

[3] D. Orfanus, F. Eliassen, and E. P. de Freitas, "Self-organizing relay network supporting remotely deployed sensor nodes in military operations," in *Proc. 6th Int. Congr. Ultra Modern Telecommun. Control Syst. Workshops (ICUMT)*, Oct. 2014, pp. 326–333.

[4] J. Colorado, I. Mondragon, J. Rodriguez, and C. Castiblanco, "Geo-mapping and visual stitching to support landmine detection using a low-cost UAV," *Int. J. Adv. Robotic Syst.*, vol. 12, no. 9, p. 125, Jan. 2015.

[5] A. K. Yadav and P. Gaur, "AI-based adaptive control and design of autopilot system for nonlinear UAV," *Sadhana*, vol. 39, no. 4, pp. 765–783, Aug. 2014.

[6] B. Zhao, B. Xian, Y. Zhang, and X. Zhang, "Nonlinear robust adaptive tracking control of a quadrotor UAV via immersion and invariance methodology," *IEEE Trans. Ind. Electron.*, vol. 62, no. 5, pp. 2891–2902, May 2015.

[7] Z. Zuo and P. Ru, "Augmented L_1 adaptive tracking control of quad-rotor unmanned aircrafts," *IEEE Trans. Aerosp. Electron. Syst.*, vol. 50, no. 4, pp. 3090–3101, Oct. 2014.

[8] Y. Jung, S. Cho, and D. H. Shim, "A trajectory-tracking controller design using L_1 adaptive control for multi-rotor UAVs," in *Proc. Int. Conf. Unmanned Aircr. Syst. (ICUAS)*, Jun. 2015, pp. 132–138.
[9] H. Bouadi, A. Aoudjif, and M. Guenifi, "Adaptive flight control for quadrotor UAV in the presence of external disturbances," in *Proc. 6th Int. Conf. Modeling, Simulation, Appl. Optim. (ICMSAO)*, May 2015, pp. 1–6.
[10] M. Abdolhosseini, Y. M. Zhang, and C. A. Rabbath, "An efficient model predictive control scheme for an unmanned quadrotor helicopter," *J. Intell. Robotic Syst.*, vol. 70, nos. 1–4, pp. 27–38, Apr. 2013.
[11] Y. Zheng, Z. Liu, and L. Liu, "Robust MPC-based fault-tolerant control for trajectory tracking of surface vessel," *IEEE Access*, vol. 6, pp. 14755–14763, 2018.
[12] M. Kamel, M. Burri, and R. Siegwart, "Linear vs nonlinear MPC for trajectory tracking applied to rotary wing micro aerial vehicles," *IFAC-PapersOnLine*, vol. 50, no. 1, pp. 3463–3469, Jul. 2017.
[13] P. Oettershagen, A. Melzer, S. Leutenegger, K. Alexis, and R. Siegwart, "Explicit model predictive control and L1-navigation strategies for fixed-wing UAV path tracking," in *Proc. 22nd Medit. Conf. Control Automat.*, Jun. 2014, pp. 1159–1165.
[14] T. J. Stastny, A. Dash, and R. Siegwart, "Nonlinear MPC for fixed-wing UAV trajectory tracking: Implementation and flight experiments," in *Proc. AIAA Guid., Navigat., Control Conf.*, 2017, p. 1512.
[15] C. Hu, Z. Zhang, Y. Tao, and N. Wang, "Decentralized real-time estimation and tracking for unknown ground moving target using UAVs," *IEEE Access*, vol. 7, pp. 1808–1817, 2018.
[16] J.-J. Xiong and E.-H. Zheng, "Position and attitude tracking control for a quadrotor UAV," *ISA Trans.*, vol. 53, no. 3, pp. 725–731, May 2014.
[17] Z. Weidong, Z. Pengxiang, W. Changlong, and C. Min, "Position and attitude tracking control for a quadrotor UAV based on terminal sliding mode control," in *Proc. 34th Chinese Control Conf. (CCC)*, Jul. 2015, pp. 3398–3404.
[18] H. Chen, K. Chang, and C. S. Agate, "UAV path planning with tangent-plus-Lyapunov vector field guidance and obstacle avoidance," *IEEE Trans. Aerosp. Electron. Syst.*, vol. 49, no. 2, pp. 840–856, Apr. 2013.
[19] Y. Liang, Y. Jia, Z. Wang, and F. Matsuno, "Combined vector field approach for planar curved path following with fixed-wing UAVs," in *Proc. Amer. Control Conf. (ACC)*, Jul. 2015, pp. 5980–5985.
[20] G. Dong and Z. H. Zhu, "Position-based visual servo control of autonomous robotic manipulators," *Acta Astronautica*, vol. 115, pp. 291–302, Oct./Nov. 2015.
[21] M. M. Aref, R. Ghabcheloo, A. Kolu, M. Hyvonen, K. Huhtala, and J. Mattila, "Position-based visual servoing for pallet picking by an articulated-frame-steering hydraulic mobile machine," in *Proc. 6th IEEE Conf. Robot., Automat. Mechatronics (RAM)*, Nov. 2013, pp. 218–224.
[22] K. Mohta, V. Kumar, and K. Daniilidis, "Vision-based control of a quadrotor for perching on lines," in *Proc. IEEE Int. Conf. Robot. Automat. (ICRA)*, May/Jun. 2014, pp. 3130–3136.
[23] H. de Plinval, P. Morin, P. Mouyon, and T. Hamel, "Visual servoing for underactuated VTOL UAVs: A linear, homography-based framework," *Int. J. Robust Nonlinear Control*, vol. 24, no. 16, pp. 2285–2308, Nov. 2014.
[24] H. Jabbari, G. Oriolo, and H. Bolandi, "An adaptive scheme for image-based visual servoing of an underactuated UAV," *Int. J. Robot. Autom.*, vol. 29, no. 1, pp. 92–104, May 2014.
[25] M. Keshmiri, W.-F. Xie, and A. Mohebbi, "Augmented image-based visual servoing of a manipulator using acceleration command," *IEEE Trans. Ind. Electron.*, vol. 61, no. 10, pp. 5444–5452, Oct. 2014.
[26] H. Xie, A. F. Lynch, and M. Jagersand, "Dynamic IBVS of a rotary wing UAV using line features," *Robotica*, vol. 34, no. 9, pp. 2009–2026, Sep. 2016.
[27] J. Thomas, G. Loianno, K. Sreenath, and V. Kumar, "Toward image based visual servoing for aerial grasping and perching," in *Proc. IEEE Int. Conf. Robot. Automat. (ICRA)*, May/Jun. 2014, pp. 2113–2118.
[28] X. Zhang, Y. Fang, and X. Liu, "Motion-estimation-based visual servoing of nonholonomic mobile robots," *IEEE Trans. Robot.*, vol. 27, no. 6, pp. 1167–1175, Dec. 2011.
[29] V. Lippiello, J. Cacace, A. Santamaria-Navarro, J. Andrade-Cetto, M. A. Trujillo, Y. R. Esteves, and A. Viguria, "Hybrid visual servoing with hierarchical task composition for aerial manipulation," *IEEE Robot. Autom. Lett.*, vol. 1, no. 1, pp. 259–266, Jan. 2016.
[30] F. Chaumette, "Visual servoing," in *Computer Vision: A Reference Guide*, K. Ikeuchi, Ed. Boston, MA, USA: Springer, 2014, pp. 869–874. doi: 10.1007/978-0-387-31439-6_281.
[31] D. Falanga, P. Foehn, P. Lu, and D. Scaramuzza, "PAMPC: Perception-aware model predictive control for quadrotors," 2018, *arXiv:1804.04811*. [Online]. Available:https://arxiv.org/abs/1804.04811
[32] P. Peliti, L. Rosa, G. Oriolo, and M. Vendittelli, "Vision-based loitering over a target for a fixed-wing UAV," *IFAC Proc. Vol.*, vol. 45, no. 22, pp. 51–57, 2012.
[33] S. A. P. Quintero and J. P. Hespanha, "Vision-based target tracking with a small UAV: Optimization-based control strategies," *Control Eng. Pract.*, vol. 32, pp. 28–42, Nov. 2014.
[34] F. Le Bras, T. Hamel, and R. Mahony, "Image-based visual servo control for circular trajectories for a fixed-wing aircraft," in *Proc. 48h IEEE Conf. Decis. Control (CDC)*, Dec. 2009, pp. 3430–3435.

LINGJIE YANG received the bachelor's degree in automation from the National University of Defense Technology, Changsha, China, in 2017, where he is currently pursuing the M.S. degree in control science and engineering. His current research interests include nonlinear control, intelligent systems, and visual servo control for UAV.

ZHIHONG LIU received the B.S. degree from the South China University of Technology, in 2009, and the M.S. and Ph.D. degrees from the National University of Defense Technology, in 2011 and 2016, respectively, all in computer science, where he is currently an Assistant Professor with the College of Mechatronic Engineering and Automation. His research interests include the coordination of multiple UAVs, UAV swarming, and visual serving.

XIANGKE WANG (M'12–SM'18) received the B.S., M.S., and Ph.D. degrees in control science and engineering from the National University of Defense Technology, Changsha, China, in 2004, 2006, and 2012, respectively.

Since 2014, he has been an Associate Professor with the College of Mechatronic Engineering and Automation, National University of Defense Technology. He has published a number of journal papers. His current research interests include coordinated decision and control of multiple UAV systems, nonlinear control, and visual servo control.

YINBO XU received the B.A. degree in automation and the master's degree in control science and engineering from the National University of Defense Technology, in 2016 and 2018, respectively. His research interests include pattern recognition and intelligent systems, and robot especially UAV control and artificial intelligence.